Gas-Phase Laser-Induced Pyrolysis of Tapered Microstructures

James Maxwell
Joseph Pegna
Eric Hill
Rensselaer Polytechnic Institute
Troy, New York

Abstract:

Gas-phase Selective Area Laser Deposition (SALD) is a useful freeform fabrication tool for the prototyping of simple three-dimensional microstructures. Using this method, slender graphite and nickel rods of various diameters were grown from ethylene and nickel tetracarbonyl, respectively. By varying the laser power during growth, tapered cone-like structures were also generated. Rod diameters and material morphology were correlated with the SALD process parameters to demonstrate the mechanisms through which steady-state rod growth occurs--and through which it can be controlled. Rods, and other similar microstructures, have many useful applications, and are preliminary building blocks for further modelling and development of the SALD process as a micromachining tool.

Keywords: *Laser chemical vapor deposition, LCVD, SALD, 3-dimensional growth, micro fabrication, rapid prototyping, micro electro mechanical systems, pyrolysis, graphite, nickel, rods, cones.*

1. Introduction

Over the past decade, laser-induced chemical vapor deposition (LCVD) has been explored extensively as a thin-film prototyping tool. Its primary application has been the direct-writing of conductive traces on custom integrated circuits and higher-level packaging [Adler, 1990; Garrido, 1989; McWilliams, 1984]. As a result, the available literature[1] focuses on the deposition of scanned metal lines on silicon and quartz substrates, usually with film thicknesses less than 5 microns. Both pyrolytic and photolytic LCVD have been studied.

In contrast, *SALD* (or 3D-LCVD) is a 3-dimensional mode of pyrolytic *LCVD*, where much taller structures can be generated, such as the rods shown in Figure 1. While the basic growth mechanism for both processes remains the same, i.e. laser-induced pyrolysis of a gaseous precursor, in 3D-LCVD the kinetics of growth cease to be determined by substrate properties, and freeform growth of deposit-on-deposit is predominant.

1. For more information on 2-dimensional LCVD and its applications, please refer to one of the following references:
(early papers) Allen, 1979; Deutsch, 1979;
(Short Reviews/important papers) Bäuerle, 1984; Ehrlich, 1984; Bäuerle, 1990; Baum, 1992;
(Books) Ehrlich, 1989

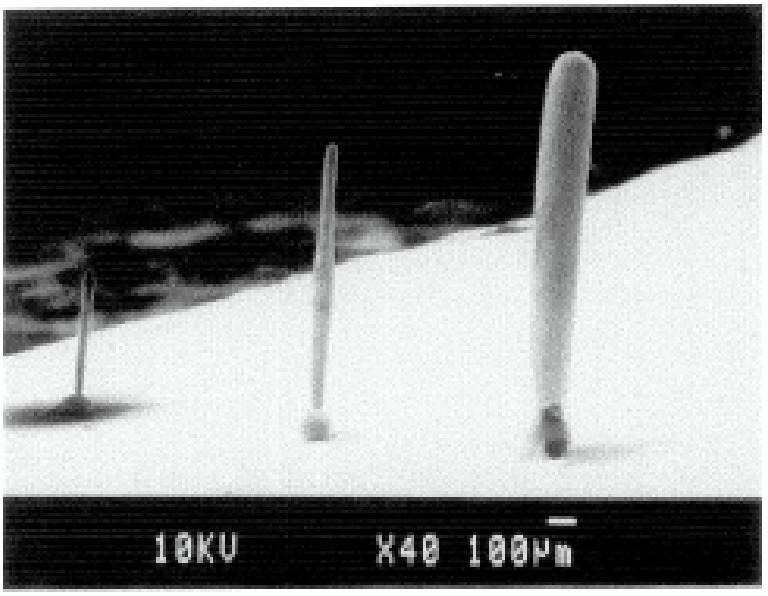

Initial Power = 6700 mW

Steady-State Power:
(Running from Left to Right)
3500 mW, 3750 mW, 4250 mW

Chamber Pressure = 550 mbar

C_2H_4 Flowrate = 175 sccm

H_2 Flowrate = 100 sccm

Fig. 1: Graphite Rods

Note that it is not always possible to grow a *3-dimensional* microstructure using an otherwise-successful thin-film LCVD process--even if the dwell-time of the scanning laser is increased without bound. Often, the deposit will only grow to a certain thickness, and then growth will cease; this is termed *self-limiting*. Usually, the thermophysical properties of the deposit determine when such height-limiting occurs. Some self-stop mechanisms are:

1. The Optical Self-stop Mechanism: absorbance of the deposit is less than that of the substrate, so that less incident power is absorbed as the film grows, thereby lowering the temperature and subsequent growth rates. Some examples of this effect can be found in the literature: [Allen, 1979; Meunier, 1992, Hopfe, 1993]

2. The Conductivity Self-stop: substrate/deposit exhibit a thermal conductivity mismatch such that it becomes progressively more difficult to laser-heat the deposit (usually a conductive deposit on a less conductive substrate.) Examples are: [Allen, 1983]

3. The Melting Self-stop: the deposit begins to evaporate/melt under the beam focus, eventually reaching an equilibrium condition with the growth process. [Westberg, 1992].

Our interest is in LCVD processes which are *not* self-limiting--a property which allows 3D-LCVD to be used as a freeform fabrication tool for micro electro mechanical systems. In this paper, we will show how the precursor partial pressure and incident laser power affect the 3-D growth of two dissimilar materials, nickel and carbon. The former has the much higher thermal conductivity--about 71.8 W/m K at 1000 K--vs. 1.3 W/m K for graphite ($\perp$ to layers).

2. Experimental

For our 3D-LCVD experiments, we constructed a system which allows growth of a variety of metals and their carbides. It consists of a reaction chamber, gas-delivery system, optics table, and laser.

The 3D-LCVD reactor consists of a custom, 50-cm long, quartz tube with several ports for viewing and laser input. The chamber is connected to a pumping station via a manual gate valve which sets the total system pressure during operation. The vacuum chamber and gas-delivery system are enclosed within a ventilated hood for safety purposes, and the quartz tube is suspended from a heavy superstructure to isolate the system from vibration.

To deliver a precursor to the vacuum system, a gas, either a reactive gas such as H_2 or a source for binary compound such as ethylene, is passed through a powder *diffuser* where solid-phase precursors are heated and sublime--or else are passed through a *bubbler* to evaporate a liquid precursor. The carrier gas and evaporated precursor subsequently pass into the reaction chamber. The ratio and quantity of gases delivered to the chamber are determined by flow meters and pneumatic switching valves. Flow meters in the system are controlled by an MKS 3-channel flow ratio controller.

Pressure measurement is made using a high-temperature, differential, capacitive manometer, attached between the reaction chamber and the high-vacuum region behind the gate valve. Absolute pressure is measured at the lower temperature, high-vacuum region by a Baratron manometer and dial gauge, allowing absolute measurement of the chamber pressure indirectly.

For the carbon deposition, pyrolysis of ethylene, C_2H_4, was used according to the overall reaction:

$$C_2H_{4(g)} \text{ --> } 2C_{(s)} + 2H_{2(g)} \qquad (1)$$

Ethylene was chosen as it adsorbs readily onto silicon and graphite at room temperature, and dissociates readily at attainable temperatures [Westberg, 1992]. It has an apparent activation energy of 78-90 kJ/mol.

For nickel deposition, a common LCVD precursor, tetracarbonyl nickel, i.e. $Ni(CO)_4$, was employed; this compound melts at -25°C, and has an ambient vapor pressure (1000 mbar) at 43°C. As a result, it is one of the fastest known precursors for LCVD; peak normal deposition rates up to 100 μm/s have been reported [Herman, 1983]. $Ni(CO)_4$ dissociates according to the reaction:

$$Ni(CO)_{4(g)} \text{ --> } Ni_{(s)} + 4(CO)_{(g)}, \qquad (2)$$

with an activation energy of 48-49 kJ/mol. The compound also decomposes at relatively low temperatures, beginning at about 150°C, and hence requires lower laser power densities to effect growth. Unfortunately, it is also rather toxic, is flammable, and must be handled within a fume hood. To supply the $Ni(CO)_4$ to the chamber without condensation, we cooled a small sample cylinder of the compound in ice water, leaving the vapor source at least 5 K below the cleanroom temperature of 20°C. Vapor pressures up to 200 mbar were possible with this setup.

In both cases, graphite substrates (Alfa/Aesar #10832) were employed, which were rinsed in acetone and isopropyl alcohol, together with a brief vacuum bake to remove water and organic residues. The graphite is a useful substrate as it has a high lateral thermal conductivity which tends to broaden the initial laser-induced growth zone. The thermal conductivity perpendicular to the graphitic layers is also very low, inhibiting conduction away from the surface layers. Finally, the substrate surface is non-specular, allowing easy visualization of the focal spot, and it provides many natural sites for nucleation.

The laser used to induce growth was a Coherent-model argon ion laser, with a maximum output of 8 W (multi-mode) at the 488/514 primary lines. At these wavelengths, pyrolytic graphite and nickel have normal spectral reflectances of approximately 0.7 and 0.6 respectively. Gaussian spot radii of 25 μm ($1/e^2$) or greater were used throughout the experiments, and it was found that while the initiation of growth on the substrate depended greatly on the power density--requiring small spot sizes for the laser powers available, the 3-D, steady-state growth of rods was affected much less by the beam waist. The optical system consisted of a Newport 10x beam expander and 200 mm focal length achromat. The theoretical spotsize of the optical system was: 5 μm, with a maximum power density of 200 mW/μm^2. To attenuate the polarized beam, a liquid-crystal polarization rotator (Newport Model #932-VIS) and beam-splitter are utilized; these are controlled by the analog output of a Macintosh computer D-A board.

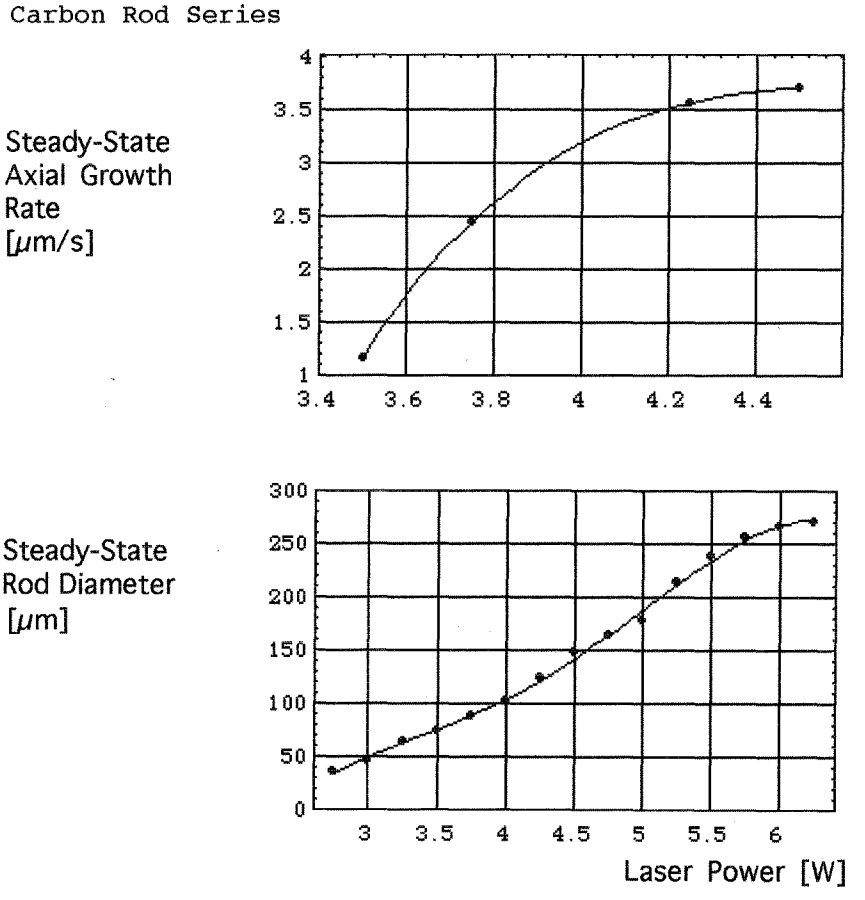

Fig. 2: Carbon Axial Rate and Rod Diameters vs. Power

3. Results

To map the growth process, we conducted a set of experiments where the process parameters (in this case the total laser power and precursor pressure) were varied while the beam remained stationary, yielding needles of various diameters and heights, such as those shown in Figure 1.

3.1 Carbon Growth

Our first objective was to characterize the growth of a moderate conductor on a substrate of similar thermal conductivity; this was the case of carbon on graphite. Preliminary results for a sequence of rods grown at constant laser powers and pressures are given in Figure 2. Note that the axial growth rate of the needles approached an asymptote of about 4 μm/s as the laser power rose to values greater than 4000 mW, indicative of mass transport limiting along the centerline. Further studies along these lines will be conducted to support this claim conclusively.

The steady-state rod diameter also varies with laser power, rising from a threshold power of about 2750 mW to a maximum diameter of about 270 μm at powers above 6500 mW. Some diffusion limiting of the radial growth rate appears to occur beginning at laser powers above 5500 mW. In all cases, the total chamber pressure was maintained at 550 mbar, while the C_2H_4 and H_2 mass flowrates were 175 sccm and 100 sccm, respectively.

Initial experiments where the chamber pressure was altered during growth (between 150 and 550 mbar) did not appear to affect the steady-state diameter of the rods greatly, although needle growth from ethylene was difficult to initiate at pressures below 150 mbar. The constant needle diameters indicate that the radial growth was primarily determined by surface temperature and reaction kinetics. However, we do not yet have an explanation for the threshold-pressure effect.

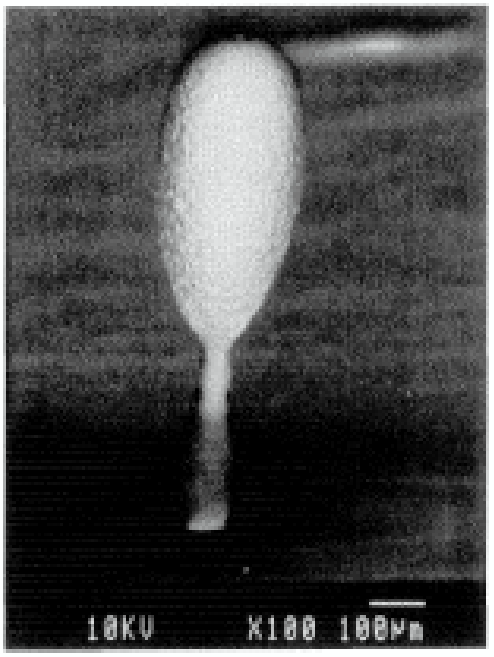

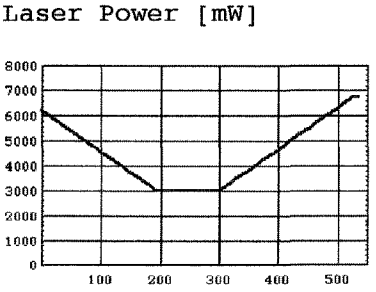

Pressure=532 mbar

C_2H_4 Flowrate=175 sccm

H_2 Flowrate=100 sccm

Fig. 3: Tapered Graphite Structure

We also attempted to grow several tapered axi-symmetric structures of graphite by varying the laser power; one such micro-shape is shown in Figure 3. Note the inset graph where the total laser power vs. time is given. One would expect an hourglass shape from the power profile, but the lower hourglass bulb was much smaller than the upper half. This is tentatively explained by the greater initial conduction to the substrate during the commencement of

growth. Data of rod diameter vs. laser power measured on the upper bulb of the tapered needle corresponds closely to the straight rod diameters given in the plot above.

3.2 Nickel Deposition

Growth of nickel microstructures proved to be more challenging than the carbon growth. While the decomposition temperature is low, facilitating rapid growth, the CO reaction by-products tended to dissociate as well, allowing solid carbon particulates to form at an amazing rate. Rapid convection past the horizontal needles was observed during growth, and the carbon particulates accumulated quickly on the substrate, often obliterating our samples.

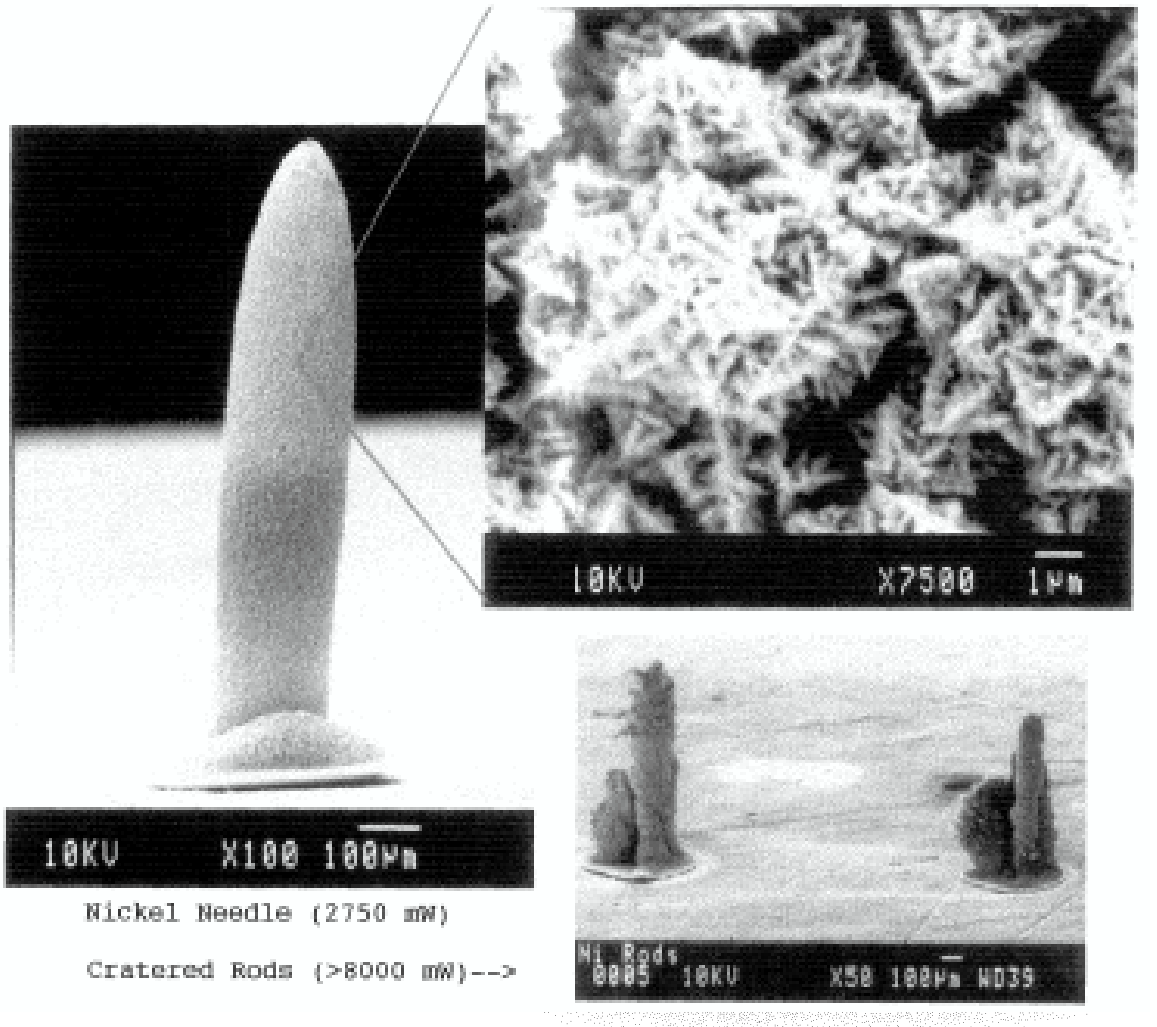

Fig. 4: Nickel Microstructures and Their Morphology

At high laser powers, crater-like structures formed rather than simple rods. This can be most likely explained by transport limitations induced by the rapid efflux of reaction products--four CO groups for every Ni atom deposited. Black *smoke* was often ejected from the focal site in bursts. The cause of the periodic bursts is unknown. At lower laser powers, smooth polycrystalline rods could be grown, such as that shown in Figure 4. The apparent grain size in the smooth needles was approximately 5 microns, the size rising rapidly above incident powers of 5000 mW.

Several important observations can be made about the growth of nickel vs. graphite. First, the nickel needles were much broader than their graphite counterparts, owning to nickel's higher thermal conductivity--a property which broadens the heated surface area over which deposition may occur. For the same reason, the initial attachment point of the nickel needles onto the substrate was very large, while the graphite rods nucleated from a small attachment zone. In addition, the lower threshold decomposition temperature of $Ni(CO)_4$ allows nucleation over a comparatively broad area.

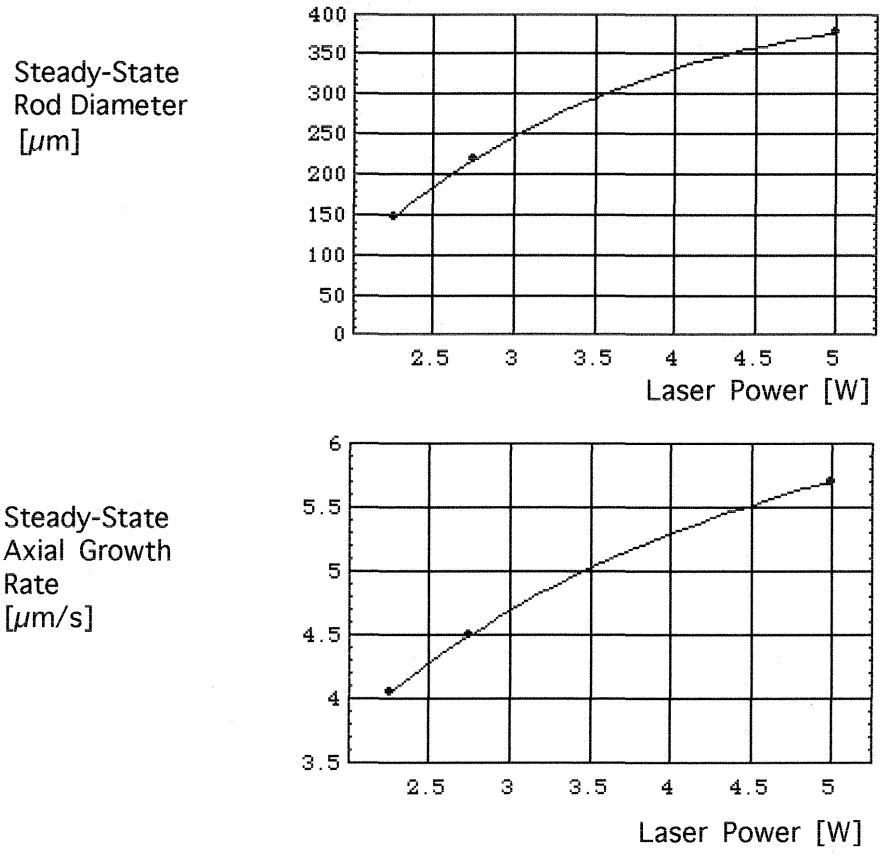

Fig. 5: Nickel Axial Rate and Rod Diameters vs. Power

$Ni(CO)_4$ vapor pressures of 200 mbar (static fill) were employed throughout the experiment, and rods could be initiated at pressures less than 25 mbar. The axial growth rate was higher than that of the ethylene-grown structures, exceeding 18 μm/s at the highest powers. The axial rate and steady-state diameter for several smooth nickel rods can be seen in Figure 5. Further data will be necessary to determine the onset of diffusion limitation and to conclusively characterize the process for shape-forming.

The purity of the deposits was determined using energy dispersive X-ray spectroscopy (EDS). Results for the smooth Ni rod shown above indicate that the percentage of carbon, oxygen, and tungsten contamination in the deposit is small, less than 0.5% in each case. Tungsten was present in the sample because $W(CO)_6$ has been previously evaporated in the system. The carbon and oxygen were left over by-products. More quantitative results will be performed later using Auger spectroscopy.

4. Conclusions

The potential of 3D-LCVD as a shape-forming process for micro mechanical parts is apparent, providing control of the transient growth near the substrate can be achieved. Continuing studies will show the effects of laser spot waist, beam intensity profile, and spot eccentricity on the initial and steady-state stages of 3-dimensional axi-symmetric growth.

Acknowledgments: Our appreciation goes to several M.S. students who helped make this project a reality, including: Dave DeAngelis, Luca Maciucescu, and Ileana Gonzalez. Thanks also to Dr. Y.S. Liu of the GE Corporate Research and Development Center for useful suggestions and technical input. This project was made possible in part by a small grant for exploratory research NSF ECS-9314071 and NSF DDM-9057059.

5. Bibliography

[Adler, 1990] Adler, M. S., SPIE Symposium on Advances in Interconnects and Packaging, Vol. 1390, Paper No. 34, (Nov. 1990).

[Allen, 1979] Allen, S. D., Bass, M., J. Vac. Sci. Technol., Vol. 16, No. 2, (Mar./Apr. 1979), p. 431.

[Baum, 1992] Baum, T. H., Comita, P. B., Thin Solid Films, Vol. 218, (1992), pp. 80-94.

[Bäuerle, 1984] Bäuerle, D., Springer Series in Chemical Physics 39, Laser Processing and Diagnostics, (1984), pp.166-182.

[Bäuerle, 1990] Bäuerle, D., Luk'yanchuk, B., Piglmayer, K., Appl. Phys. A, Vol. 50, (1990), p. 385-396.

[Deutsch, 1979] Deutsch, T. F., Ehrlich, D. J., Osgood, R. M., Jr., Appl. Phys. Lett., Vol. 35, No. 2, (15 Jul. 1979), pp. 175-177.

[Ehrlich, 1984] Ehrlich, D. J., Tsao, J. Y., Appl. Phys. Lett., Vol. 44, No. 2, (15 Jan. 1984), pp. 267-269.

[Ehrlich, 1989] Edited by: Ehrlich, D. J., Tsao, J. Y., Laser Microfabrication, Thin Film Processes and Lithography, Academic Press, (1989), pp. 385-429.

[Garrido, 1989] Garrido, C., Braichotte, D., Van Den Bergh, H., León, B., Pérez-Amor, M., Applied Surface Science, Vol. 43, (1989), pp. 68-73.

[Herman, 1983] Herman, I. P., Hyde, R. A., McWilliams, B. M., Weisberg, A. H., Wood, L. L., Materials Research Society Symposium Proceedings, Vol. 17, (1983), p. 9.

[Hopfe, 1993] Hopfe, V., Böhm, S., Wieghardt, G., Schulze, A., Applied Surface Science, Vol. 69, (1993), pp. 380-387.

[Meunier, 1992] Meunier, M., Izquierdo, R., Desjardins, P., Tabbal, M., Lecours, A., Yelon, A., Thin Solid Films, Vol. 218, (1992), pp. 137-143.

[McWilliams, 1984] McWilliams, B. M., Chin, H. W., Herman, I. P., Hyde, R. A., Mitlitsky, F., Whitehead, J. C., Wood, L. L., Proceedings Of SPIE-The International Society for Optical Engineering, Laser Assisted Deposition, Etching, and Doping, Vol. 459, (1984), pp.49-54.

[Westberg, 1992] Westberg, H., Boman, M., Norekrans, A.-S., Carlsson, J.-O., Thin Solid Films, Vol. 215, (1992), pp. 126-133.